Exchange bias in epitaxial CoO/Co bilayers with different crystallographic symmetries

Tomasz Blachowicz
Department of Electron Technology, Institute of Physics, Silesian University of Technology, Krzywoustego 2, 44100 Gliwice, Poland

Andrea Tillmanns
FTB, Niederrhein University of Applied Sciences, Webschulstraße 31, 41065 Mönchengladbach, Germany

Michael Fraune, Reza Ghadimi, Bernd Beschoten, and Gernot Güntherodt
II. Physikalisches Institut, RWTH Aachen, 52056 Aachen, Germany

(Received 13 October 2006; revised manuscript received 29 December 2006; published 28 February 2007)

The magnetic anisotropies of epitaxially grown exchange bias CoO/Co bilayers with (111), (110), and (100) crystallographic orientations have been investigated by Brillouin light scattering (BLS) by means of spin waves. Experiments were carried out at 293 and 140 K, i.e., above and below, respectively, the Néel temperature of CoO. The unidirectional, twofold, and fourfold anisotropy constants, bulk and surface, were obtained by fitting the angular dependence of the spin wave frequencies. For all samples, we observed an isotropic up-shift of the spin wave frequencies. We conclude that all observed magnetic anisotropies are related to the crystallographic symmetry of the ferromagnetic and antiferromagnetic layers, depending on the lattice mismatch between layers, the sequence of layers upon deposition, and the quality of the ferromagnetic/antiferromagnetic interface.

DOI: 10.1103/PhysRevB.75.054425 PACS number(s): 75.30.Gw, 78.35.+c, 75.75.+a, 85.25.Dq

I. INTRODUCTION

The phenomenon of exchange bias (EB) in coupled ferromagnetic (FM) and antiferromagnetic (AFM) thin films is characterized by a hysteresis loop shift along the field axis and an enhancement of the coercive field. This effect attracted attention due to practical applications in magnetoelectronics, for example in spin valves or giant magnetoresistance devices.[1–4] Since the discovery of EB by Meiklejohn and Bean in 1956,[5] a wealth of results has been obtained in different experiments.[6–8] Lately, it has been shown that this interfacial phenomenon can be tailored by creating a specific domain state in a volume part of the AFM.[9–11] Physically, this state can be obtained by nonmagnetic substitution or vacancy creation at magnetic sites of the AFM during its epitaxial growth, or by the use of ion-beam irradiation that modifies the material structure[12] or influences energy levels of antiferromagnetic grains and domains, thus acting as a local hyperthermal heating.[13,14] Exchange biased bilayers have to be cooled below the Néel temperature T_N of the AFM in a presence of a magnetic field (the field-cooling process).

Additionally, by a proper choice of substrate orientation and growth conditions, it is possible to obtain FM/AFM bilayers with FM layers exhibiting different symmetries of in-plane anisotropies. This has consequences for the angular dependence of the spin wave frequencies measured in Brillouin light scattering (BLS) experiments.

What follows are detailed results of BLS measurements from spin waves in MgO(110)/Co/CoO, MgO(110)/CoO/Co, and MgO(100)/CoO/Co samples used to test the induced magnetic in-plane anisotropies of fourfold, twofold, and unidirectional (exchange-bias) symmetries. We discuss the influence of the exchange bias field on bulk and surface anisotropies, especially, the influence on the anisotropies stability. The samples were also measured by superconducting quantum interferometry (SQUID) and by the high energy electron diffraction (RHEED) method. This yielded information about how magnetic anisotropies and coercivity fields were influenced by the crystallographic symmetry in a volume part of materials and about the crystallographic order at the FM/AFM interface.

We report that, for all samples after field-cooling below T_N, magnetic anisotropies were modified in such a way that the spin wave frequencies were up-shifted independently from the in-plane orientation. This is analogous to the phenomenon, observed in ferromagnetic resonance experiments (FMR) in polycrystalline exchange biased samples, described by the rotatable anisotropy.[15,16]

II. EXPERIMENT

For samples grown epitaxially on the MgO(110) and MgO(100) substrates (5×10 mm^2), the $Co_{1-y}O$ layers were diluted ($y\neq 0$) applying the oxygen partial pressure of 5×10^{-6} mbar in the UHV MBE chamber. For the sample prepared with the MgO(110)/Co(6 nm)/CoO(20 nm) layer sequence, the 6 nm fcc Co(110) was followed by a 20 nm twinned CoO(110) layer. The CoO twinning in samples checked by RHEED was visualized as two sublattices. The reversed sequence in the MgO(110)/CoO(20 nm)/Co(6 nm) sample resulted in untwinned CoO(110) and fcc structure of Co. The MgO(100)/CoO(20 nm)/Co(10 nm) sample showed untwinned CoO(110) and hcp-Co with the c axis lying in the sample plane. On a top surface of samples several monolayers of Au were deposited to avoid oxidation.

During deposition of all layers, no external magnetic field was applied, since field cooling was easily achieved with $T_N=291$ K. To provide a broader viewpoint, the BLS spectrum of the Si(111)/Co(8 nm)/CoO(50 nm) sample measured in previous experiments is also reported here.[17] In this

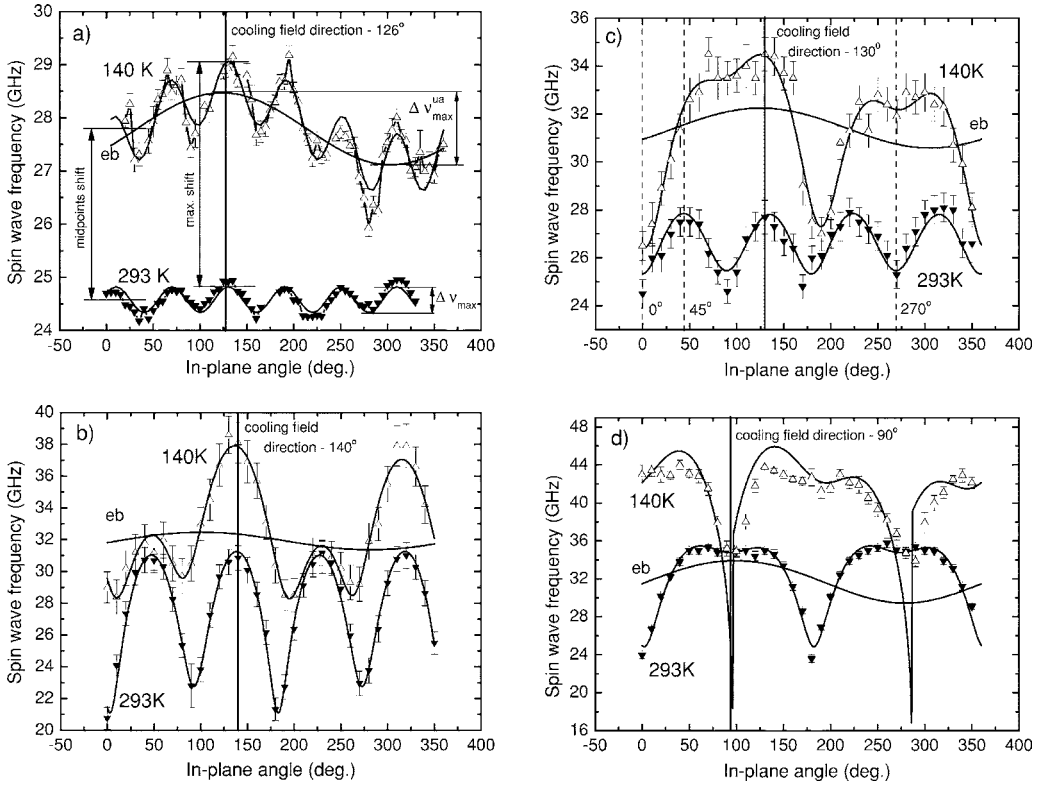

FIG. 1. Brillouin light scattering measurements in samples of different anisotropy field symmetries resulting from deposition conditions: (a) Si(111)/Co(8 nm)/CoO(50 nm) sample (Ref. 17) (b) MgO(100)/CoO(20 nm)/Co(10 nm) sample, (c) MgO(110)/Co(6 nm)/CoO(20 nm) sample—the SQUID cooling field directions are marked by 0°, 45°, and 270° for a convenience, (d) the MgO(110)/CoO(20 nm)/Co(6 nm) sample, where the easy and hard axes of magnetization at room temperature were perpendicularly switched after the field cooling to 140 K—the SQUID cooling field directions were 0° and 90° in this case. In the figures the exchange bias (EB) $(2/d)k_{EB}\cos(\phi-\phi_{EB})$ anisotropy contribution (least squares fitting) is shown separately.

case, the Co layer had an (111) orientation, the CoO(111) layer was twinned and the sample possessed a dominating sixfold in-plane anisotropy symmetry.

Brillouin light scattering (BLS) measurements[18] were performed using a Sandercock tandem three-pass spectrometer,[19] and an Ar^+ ion laser working at a wavelength of 514.5 nm in the back-scattering geometry. The external dc magnetic field was applied in a sample plane and perpendicular to the scattering plane, which was the plane of the laboratory table, in order to induce spin waves propagating on a sample surface. The low temperature measurements (140 K) were carried out in a glass cryostat with a cold finger in a vacuum of 2×10^{-6} mbar. The temperature was stabilized within an accuracy of ±0.1 K. The sample was rotated in-plane in the range of 0°–350° with a step of 10°. The experimental error of the spin wave frequency values was affected by the accuracy of reading a peak position, using a Lorentz-type shape fitting, and by an uncertainty derived from the accuracy of the optical alignment of the experimental arrangement. This uncertainty did not exceed 2%.[20] The measurements at 293 and 140 K were carried out in a magnetic field of 0.4 T, which was also the value of the cooling field. The cooling field directions were chosen near the maximum values of the spin wave frequencies, i.e., parallel to the magnetic easy axes.

The results of the BLS measurements are depicted in Fig. 1(a) for the Si(111)/Co/CoO sample,[17] in Fig. 1(b) for MgO(100)/CoO/Co, in Fig. 1(c) for MgO(100)/Co/CoO, and in Fig. 1(d) for MgO(110)/CoO/Co, exhibiting at 293 K, respectively, sixfold, dominating fourfold, fourfold and twofold, and dominating twofold, symmetries in the angular dependence on spin wave frequency. In all cases we measured the frequency of the Damon Eshbach[21] (DE) mode propagating on the Co surfaces. The symmetries of the angular dependence of the spin waves at 293 and 140 K were confirmed by fits shown by the solid lines in Figs. 1(a)–1(d).

Also, an additional onefold (unidirectional) symmetry appeared in the measurements at 140 K. The unidirectional symmetry, marked in figures by *eb*, was also deduced from the fits and is shown separately. After cooling to 140 K we observe an overall, isotropic up-shift of the spin wave frequencies and changes of all anisotropies.

A rough comparison between the room and low-temperature data, especially the relation between the amplitudes of the angular variation and the up-shift of spin wave frequency, obtained after field cooling, suggests that there is some trend in these results (Table I). The sixfold (111) CoO/Co system[17] at 293 K in Fig. 1(a) has maximum frequency variations of 0.5 GHz, while the resultant frequency up-shift between 293 and 140 K equals about 4.2 GHz, when

TABLE I. The up-shifts of maximum values of spin wave frequencies in the field cooling direction, the up-shift readout between the midpoint of the room temperature data and the midlevel of the unidirectional contribution, the amplitude of frequency variations at room temperature $\Delta\nu_{\max}$ and the amplitude of the unidirectional anisotropy frequency variations at 140 K $\Delta\nu^{ua}_{\max}$ (140 K) [companion descriptions in Fig. 1(a)]. The data are taken from the fitted curves. The frequency uncertainty is equal to 0.1 GHz.

Sample	Shift of maxima (GHz)	Midpoint shift (GHz)	$\Delta\nu_{\max}$ (GHz)	$\Delta\nu^{ua}_{\max}$ (140 K) (GHz)
MgO(100)/CoO/Co	7.1	6.0	8.7	1.1
MgO(110)/Co/CoO	6.8	5.1	1.9	1.6
MgO(110)/CoO/Co	7.5[a]	1.7	10.0	4.4
Si(111)/Co/CoO[17]	4.2[b]	3.3	0.5	1.4

[a]The shift between 293 K data and the maximum values of the switched easy direction at 140 K.
[b]For similar MgO(111)/Co/CoO sample the measured shift was equal to 4.1±0.8 GHz.

comparing maximum values of the fitted data in the field cooling direction. Similarly, the frequency shift taken along the cooling field direction, between the midpoint of the frequency variations at 293 K and the midpoint of the frequency variation of the unidirectional contribution at 140 K, is equal to 3.3 GHz. We can use these frequency parameters to establish a trend in the magnitude of the observed frequency up-shifts of all samples. The last column in Table I provides the frequency measure of exchange-bias field.

An interesting behavior has also been found for the MgO(110)/CoO/Co sample. In the sample we observed, after a field cooling, the nearly perpendicular switching of the easy axis of magnetization. This effect can be interpreted in terms of the perpendicular coupling between FM and AFM layers as observed in epitaxial NiFe/FeMn (Ref. 22) and in polycrystalline/textured Fe/FeF_2(110) (Refs. 23 and 24) exchange biased systems. This and other symmetry modifications are discussed below.

III. DISCUSSION. STRUCTURAL DETAILS AND DATA FITTING

In order to determine anisotropy constants, a numerical procedure was applied to the data of Figs. 1(b)–1(d). The applied fitting was based on the least-squares nonlinear regression analysis according to the formula of the Damon-Eshbach in-plane spin-mode frequency

$$\omega_{\mathrm{DE}} = \gamma\left(\left[\frac{1}{M_s}\frac{\partial^2 E_{\mathrm{ani}}}{\partial^2\theta} + \frac{2A}{M_s}q^2 + 4\pi M_s f\left(1-\frac{1}{2}q_{\mathrm{II}}d\right) + H\cos(\phi-\phi_H)\right]\times\left[\frac{1}{M_s}\frac{\partial^2 E_{\mathrm{ani}}}{\partial\phi^2} + \frac{2A}{M_s}q^2 + 4\pi M_s f\frac{1}{2}q_{\mathrm{II}}d\sin^2(\phi-\phi_q) + H\cos(\phi-\phi_H)\right] - \left(\frac{1}{M_s}\frac{\partial^2 E_{\mathrm{ani}}}{\partial\theta\partial\phi}\right)^2\right)^{1/2}, \tag{1}$$

where γ is the gyromagnetic ratio, M_s is the magnetization at saturation, E_{ani} is the free energy density, A is the exchange stiffness constant, q^2 is the squared wave vector of a spin wave, f is the demagnetization factor which controls the balance between shape and magnetoelastic anisotropies (including out-of-plane contributions), q_{II} is the in-plane component of a spin-wave wave vector derived from a BLS scattering geometry, H is the externally applied magnetic field intensity, $(\phi-\phi_H)$ is the angle between external magnetic field vector $\vec{H}$ and the magnetization $\vec{M}$, and $(\phi-\phi_q)$ is the angle between the $\vec{q}$ wave vector and the magnetization $\vec{M}$. The four components, seen in the first and the second squared brackets in Eq. (1), form an effective magnetic field acting on the magnetization vector $\vec{M}$. There are, respectively, from left to right, the anisotropy energy field, the exchange energy field, the demagnetization energy field, and the Zeeman energy field. We assumed the following constant values in Eq. (1): $\gamma=(1/2)\gamma_e g$, where the $\gamma_e=-1.759\times10^7$ Hz/Oe is the free electron gyromagnetic ratio, and $g=2.2$ is the spectroscopic splitting factor, $A=3\times10^{-11}$ J/m, and $4\pi M_s=17.8$ kOe.

The fitting was based on the following expressions for the free energy density:

$$\begin{aligned} E^{(100)}_{\mathrm{ani}} &= \underbrace{K^{\mathrm{hcp}}_1\sin^2(\phi-\phi_{\mathrm{hcp}}) + K^{\mathrm{hcp}}_2\sin^4(\phi-\phi_{\mathrm{hcp}})}_{\text{volume anisotropy}} \\ &\quad \underbrace{-K^{(1)}_{ME}\cos^2\theta + K^{(2)}_{ME}\cos^2(\phi-\phi_{\mathrm{ref}})\sin^2\theta}_{\text{magnetoelastic anisotropy}} \\ &= K^{\mathrm{hcp}}_1\sin^2(\phi-\phi_{\mathrm{hcp}}) + K^{\mathrm{hcp}}_2\sin^4(\phi-\phi_{\mathrm{hcp}}) \\ &\quad + K^{(2)}_{ME}\cos^2(\phi-\phi_{\mathrm{ref}})\ (\theta=90^\circ) \end{aligned} \tag{2a}$$

for the MgO(100)/CoO/Co sample at 293 K and with the $\theta=90°$ assumption (only in-plane contributions), that was kept for all considered cases in Eqs. (2a)–(4b), we have

$$E_{\mathrm{ani}}^{(100)} = \underbrace{K_1^{\mathrm{hcp}} \sin^2(\phi - \phi_{\mathrm{hcp}}) + K_2^{\mathrm{hcp}} \sin^4(\phi - \phi_{\mathrm{hcp}})}_{\text{volume anisotropy}} + \underbrace{K_{ME}^{(2)} \cos^2(\phi - \phi_{\mathrm{ref}})}_{\text{magnetoelastic anisotropy}} + \underbrace{\frac{2}{d} k_{EB} \cos(\phi - \phi_{EB})}_{\text{exchange bias}} \tag{2b}$$

for the MgO(100)/CoO/Co sample at 140 K,

$$E_{\mathrm{ani}}^{(110)} = \underbrace{\frac{1}{4} K_1^{\mathrm{fcc}} \sin^2(\phi - \phi_{\mathrm{fcc}})[1 + 4\cos^2(\phi - \phi_{\mathrm{fcc}})]}_{\text{volume anisotropy}} + \underbrace{K_{ME}^{(2)} \cos^2(\phi - \phi_{\mathrm{ref}})}_{\text{magnetoelastic anisotropy}} \tag{3a}$$

for the MgO(110)/Co/CoO sample at 293 K,

$$E_{\mathrm{ani}}^{(110)} = \underbrace{\frac{1}{4} K_1^{\mathrm{fcc}} \sin^2(\phi - \phi_{\mathrm{fcc}})[1 + 4\cos^2(\phi - \phi_{\mathrm{fcc}})]}_{\text{volume anisotropy}} + \underbrace{\frac{2}{d} k_p^{(\mathrm{twofold})} \cos^2(\phi - \phi_{(\mathrm{twofold})})}_{\text{interface anisotropy}} + \underbrace{\frac{2}{d} k_{EB} \cos(\phi - \phi_{EB})}_{\text{exchange bias}} \tag{3b}$$

for the MgO(110)/Co/CoO sample at 140 K,

$$E_{\mathrm{ani}}^{(110)} = \underbrace{\frac{1}{4} K_1^{\mathrm{fcc}} \sin^2(\phi - \phi_{\mathrm{fcc}})[1 + 4\cos^2(\phi - \phi_{\mathrm{fcc}})]}_{\text{volume anisotropy}} + \underbrace{\frac{2}{d} k_p^{(\mathrm{twofold})} \cos^2(\phi - \phi_{(\mathrm{twofold})})}_{\text{interface anisotropy}} \tag{4a}$$

for the MgO(110)/CoO/Co sample at 293 K, and

$$E_{\mathrm{ani}}^{(110)} = \underbrace{\frac{1}{4} K_1^{\mathrm{fcc}} \sin^2(\phi - \phi_{\mathrm{fcc}})[1 + 4\cos^2(\phi - \phi_{\mathrm{fcc}})]}_{\text{volume anisotropy}} + \underbrace{\frac{2}{d}[k_p^{(\mathrm{twofold})} \cos^2(\phi - \phi_{(\mathrm{twofold})}) + k_p^{(\mathrm{fourfold})} \cos^2(\phi - \phi_{(\mathrm{fourfold})}) \cos^2(\phi - \phi_{(\mathrm{fourfold})})]}_{\text{interface anisotropy}} + \underbrace{\frac{2}{d} k_{EB} \cos(\phi - \phi_{EB})}_{\text{exchance bias}} \cong K_{\mathrm{eff}}^{(\mathrm{fourfold})} \sin^2\phi \cos^2\phi + K_{\mathrm{eff}}^{(\mathrm{twofold})} \sin^2\phi + \frac{2}{d} k_{EB} \cos(\phi - \phi_{EB}), \tag{4b}$$

where

$$K_{\mathrm{eff}}^{(\mathrm{fourfold})} \approx K_1^{\mathrm{fcc}} + \frac{2}{d} k_p^{(\mathrm{fourfold})}, \quad K_{\mathrm{eff}}^{(\mathrm{twofold})} \approx \frac{1}{4} K_1^{\mathrm{fcc}} + \frac{2}{d} k_p^{(\mathrm{twofold})} \tag{4c}$$

for the MgO(110)/CoO/Co sample at 140 K. In Equations (2a)–(4c) ϕ is the in-plane rotation angle of the sample relative to: the magnetic easy axis directions ϕ_{hcp} and ϕ_{fcc} of volume anisotropies, next, $\phi_{(\mathrm{twofold})}$ and $\phi_{(\mathrm{fourfold})}$ are the easy directions of the twofold and the fourfold surface anisotropies, respectively, ϕ_{ref} is the crystallographic reference direction, here $\phi_{\mathrm{ref}} \approx 0$, and ϕ_{EB} is the direction of the unidirectional exchange-bias anisotropy. All mentioned anisotropy direction were used as additional parameters during fitting. This supported distinction between components of a similar angular dependence. Next, K_1^{hcp} and K_2^{hcp} are the hexagonal volume anisotropy constants, K_1^{fcc} is the cubic volume anisotropy constant, $K_{ME}^{(1)}$ and $K_{ME}^{(2)}$ are the magnetoelastic anisotropy constants of the first and second order, respectively, $k_p^{(\mathrm{twofold})}$ and $k_p^{(\mathrm{fourfold})}$ are the surface (FM/AFM interface) anisotropy constants of the twofold and fourfold symmetry, respectively, k_{EB} is the exchange-bias unidirectional anisotropy constant, and d is the magnetic layer thickness. The effective $K_{\mathrm{eff}}^{(\mathrm{fourfold})}$ and $K_{\mathrm{eff}}^{(\mathrm{twofold})}$ anisotropy constants were introduced for the MgO(110)/CoO/Co sample at 140 K, as it was not possible to distinguish between surface anisotropies and volume contribution for a single sample with only one value of the FM layer thickness.

For the samples grown on the MgO(100) and MgO(110) we used the fitting procedure terms with the in-plane anisotropy contributions, assuming $\theta = 90°$, however, we cannot exclude the influence of out-of-plane anisotropies. This perpendicular influence is controlled by the demagnetizing factor $f < 1$ and consequently by a magnetoelastic energy $K_{ME}^{(2)} \sin^2\theta \cos^2\phi$. Since $\theta = 90°$ the $K_{ME}^{(2)}$ gives an additional contribution by rotating the magnetization into the subsequent easy in-plane direction. In other words it was not possible to apply $K_{ME}^{(2)} \sin^2\theta \cos^2\phi$ term during fitting as f reached the maximum value, $f = 1$. It should be noted also that the sixfold case, grown on the Si(111) substrate, revealed the out-of-plane anisotropy component resulting from the 8° out-of-plane orientation of the antiferromagnetic moments in the CoO(111).[25] In this case, the measured unidi-

TABLE II. Anisotropy constants of the MgO(100)/CoO/Co sample obtained from the BLS measurements at 293 and 140 K. Below each value of the anisotropy constant, in brackets, the subsequent value of a given easy anisotropy axis position is provided (in deg.).

Temp.	K_1^{hcp} (10^4 J/m^3) (ϕ_{hcp})	K_2^{hcp} (10^4 J/m^3) (ϕ_{hcp})	$K_{ME}^{(2)}$ (10^4 J/m^3) ($\phi_{ref}\approx 0$)	f	$(2/d)k_{EB}$ (10^4 J/m^3) (ϕ_{EB})
293 K	−9.0±0.7 (357.2±0.3)	11.3±0.3 (357.2±0.3)	16.4±3.3	0.6259±0.0103	
140 K	−1.0±0.4 (222.8±0.8)	6.4±0.3 (222.8±0.8)	6.9±3.1	0.9336±0.0117	2.1±0.5[a] (101±3)

[a] $k_{EB}=(10.5\pm0.2)\times10^{-5}$ J/m^2.

rectional anisotropy constant $(2/d)k_{EB}$ was equal to $(2.5\pm0.2)\times10^4$ J/m^3 (140 K).[17] Below are some facts that explain the structural origin of anisotropies.

Thus, for the (100) symmetry sample, the MgO(100)/CoO/Co cobalt was grown in the hcp structure in the [2-1-1 0] direction. It means that the hexagon-prism c-axis was oriented in the sample plane. Also, the c-axis edge of the hexagon prism, built from Co atoms, was epitaxially immersed in the Co/CoO interface, in the last layer of CoO, between oxygen atoms. This contributed to the twofold anisotropy symmetry. Additionally, an analysis of RHEED pattern indicated the existence of two types of the Co domains oriented perpendicularly in a sample plane that resulted in a fourfold anisotropy symmetry. Also, as obtained from the RHEED, the values of the c-axis length and the length of the line perpendicular to the c axis, both lying in the sample plane, were equal to 0.434t and 0.407 nm, respectively. Thus, the c/a ratio was equal to 1.066. All this provided a hint for using the typical expression for the bulk anisotropy energy for the hexagonal (hcp) structure, using the K_1^{hcp} and the K_2^{hcp} anisotropy constants, and additionally, using the $K_{ME}^{(2)}$ magnetoelastic anisotropy contribution.[26]

Next, for the (110) symmetry samples, an initial reason for the observed anisotropy fields is the crystallographic mismatch between CoO, Co, and MgO materials. The lattice constant for CoO measured along the [100] direction is equal to 0.427 nm, and for MgO, measured along the same direction, is equal to 0.421 nm.[27] However, the same parameter measured for fcc-Co is equal to 0.3545 nm.[28] MgO and CoO are nearly matched with 1–2% accuracy, while Co shows the 18% lattice mismatch with CoO. Next, the bulk CoO usually possesses a NaCl-type structure above $T_N=291$ K. However, it is known from the RHEED analysis of CoO (below T_N) that a small tetragonal contraction and a triclinic contribution are possible.[29,30] For cobalt layers, the growth conditions of thin layers enforced the Co-fcc symmetry, while the normally bulk Co possesses a stable structure of hcp-type symmetry. This is why, during the cobalt layer deposition Co on the fcc-CoO(100) layer, we could obtain a metastable fcc-Co phase. Also, it is known that Co exhibits the fcc-phase above 723 K,[31] while Co in the MgO(110)/CoO(110)/Co(110) sample was deposited at 500 and 600 K in the MgO(110)/Co(110)/CoO(110) sample. After the preparation process both samples where cooled to ambient temperatures. Thus, it seems probable that at room temperature or below, there exists a tendency for a Co-fcc to Co-hcp phase transition. The measured ratio of the two c/a is equal to 0.9887 at 77 K for fcc phase.[28] Thus, even if this factor is relatively small, it could influence magnetic anisotropies in Co layers, and especially, contribute to a metastable behavior. Also, the measured RHEED patterns for both samples, grown on the MgO(110) substrate, gave some hints to structural FM/AFM interface details. For the MgO(110)/Co(110)/CoO(110) sample, the Co(100) distortions oriented along the [001] directions were observed. These distortions were several monolayers in height and were located near the Co/CoO interface. Similar CoO(100) distortions were visible in the MgO(110)/CoO(110)/Co(110) structure. Importantly, they were also located near the CoO/Co interface. It seems that these (100) distortions are responsible for the twofold and fourfold surface anisotropies obtained. Thus, we conclude—based on the above information for the (110) symmetry samples—that the tetragonal/monoclinic CoO distortion, the lattice mismatch between the Co and CoO layers, and the interface (100) directional distortions influenced the anisotropy symmetries and behavior. More especially, these were responsible for the nearly perpendicular switching of the easy and hard axes of magnetization for the MgO(110)/CoO/Co sample.

More hints to the surface anisotropy analysis can be found looking at the values of anisotropy constants (Tables II–IV). First, the exchange bias field can reduce or enhance other anisotropy fields. For the MgO(100)/CoO/Co sample, all the anisotropy constants were reduced. Similarly, for the MgO(110)/Co/CoO sample, all the anisotropy constants were reduced after a field-cooling process. However, the MgO(110)/CoO/Co sample, which exhibited the drastic magnetization change in the orientations of the easy and hard axes, revealed an increase of all anisotropy constants. In this case, the unidirectional anisotropy is the greatest. Second, the exchange bias field can rotate anisotropy easy axes. This occurred for the MgO(100)/CoO/Co sample, where the ϕ_{hcp} easy-axis changed its orientation from 357.2° to 222.8°. Third, a larger exchange-bias was obtained in samples with less magnetoelastic energy.

It can be said generally, that the observed anisotropy field variations are controlled by ferromagnetic domain reorientations, also locally by the spin-orbit coupling, thus, by the magnetocrystalline interactions, and equally, by the antiferromagnetic domain state. Nevertheless, all the mentioned an-

TABLE III. Anisotropy constants of the MgO(110)/Co/CoO sample obtained from the BLS measurements at 293 and 140 K. Below each value of the anisotropy constant, in brackets, the subsequent value of a given anisotropy easy axis position is provided (in deg.).

Temp.	K_1^{fcc} (10^4 J/m^3) (ϕ_{fcc})	$(2/d)k_p^{(twofold)}$ (10^4 J/m^3) ($\phi_{(twofold)}$)	$K_{ME}^{(2)}$ (10^4 J/m^3) ($\phi_{ref} \approx 0$)	f	$(2/d)k_{EB}$ (10^4 J/m^3) (ϕ_{EB})
293 K	−3.8±0.3 (0.8±1.3)		13.2±2.3	0.6349±0.009	
140 K	−3.6±0.5 (355.7±1.8)	−0.43±0.03[b] (170±2)		0.9810±0.0072	3.0±0.5[b] (125±2)

[a] $k_p^{(twofold)} = (1.3 \pm 0.1) \times 10^{-5}$ J/m^2.
[b] $k_{EB} = (9.0 \pm 1.5) \times 10^{-5}$ J/m^2.

isotropy field modifications cause an increase of the samples total-energy: spin-waves frequencies from BLS spectra were up-shifted after the field-cooling to 140 K.

To complete the experiments, the SQUID measurements were carried out for the MgO(110)/CoO/Co and MgO(110)/Co/CoO samples in order to confirm the 90° switching of the easy and hard axes of magnetization, and also to confirm appropriate modification of coercive fields. Figures 2 and 3 provide the SQUID hysteresis loops of the MgO(110)/Co/CoO and MgO(110)/CoO/Co samples, respectively. The data seem to be complementary to the BLS results and are very helpful for the subsequent interpretation. The MgO(110)/CoO/Co sample, which revealed the switching, was field cooled at 295 K along the hard (0°) and easy (90°) axes [Fig. 3(a)]. This resulted, at 140 K [Fig. 3(b)], in the reversal of the hard and easy axes. At the same time the coercivities of the easy and hard axes increased. Changes in the coercivity values were also observed for the fourfold MgO(110)/Co/CoO sample upon cooling to 140 K [Figs. 2(a) and 2(b)]. We can conclude from Fig. 2(b) that the largest changes of coercivity are observable for the 270° field cooling orientation, which is the same as the hard axis orientation at room temperature. Thus, the effect of coercivity changes is qualitatively similar to but much weaker than that for the MgO(110)/CoO/Co sample for which coercivity changes were larger.

The last issue in this paper that should be commented is the observed up-shift of the frequencies, the same for all in-plane directions, which eventually indicates the so-called rotatable anisotropy. This interesting phenomenon was observed by McMichael *et al.* in polycrystalline exchange-biased samples measured in ferromagnetic resonance (FMR) experiments.[15,16,32] In the experiments, carried out near the 10 GHz resonance, the easy axis of the AFM spins followed the movement of the ferromagnetic magnetization independently from imposed static anisotropies. It was argued that this rotatable phenomenon points to the existence of the AFM regions which are reversible at GHz frequencies—providing an angle-independent degree of freedom for the exchange-biased sample energy. Significantly, in polycrystalline samples, the rotatable anisotropy results from the existence of grains and grain boundaries at the FM/AFM interface and can be tailored mainly by the unidirectional anisotropy field. Thus, it can be said that, in the BLS experiments done at the 10^{-10} s time scales, for spin-wave frequencies at 20 GHz, the easy axis of the AFM had to overcome energy barriers resulting from the AFM partial domain walls and from anisotropy fields in the FM region. Thus, to understand the physical origin of this angle-independent anisotropy, we should eventually think about the time scales at which anisotropies are measured. Obviously, the BLS frequency up-shift was influenced and quantatively described by the exchange-bias field and other anisotropy fields expressed in terms of anisotropy constants.

We have shown then, that all types of anisotropies observed in epitaxial materials have their origin in magnetocrystalline symmetries resulting from spin-orbit coupling. More particularly, the structural factors influencing the experimental observations of exchange bias and other aniso-

TABLE IV. Effective anisotropy constants of the MgO(110)/CoO/Co sample obtained from the BLS measurements at 293 and 140 K. Below each value of the anisotropy constant, in brackets, the subsequent value of a given anisotropy easy axis position is provided (in deg.).

Temp.	K_1^{fcc} (10^4 J/m^3) (ϕ_{fcc})	$(2/d)k_p^{(twofold)}$ (10^4 J/m^3) ($\phi_{(twofold)}$)	$K_{eff}^{(fourfold)}$ (10^4 J/m^3) ($\phi_{(fourfold)} \approx 0$)	$K_{eff}^{(twofold)}$ (10^4 J/m^3) ($\phi_{(twofold)} \approx 0$)	f	$(2/d)k_{EB}$ (10^4 J/m^3) (ϕ_{EB})
293 K	−5.8±0.4 (357±1)	0.70±0.03[a] (178±1)			1.040±0.01 ≈1	
140 K			−16.4±1.3	−32.5±1.2	1	8.1±2.8[b] (99±2)

[a] $k_p^{(twofold)} = (2.1 \pm 0.1) \times 10^{-5}$ J/m^2.
[b] $k_{EB} = (24.3 \pm 8.4) \times 10^{-5}$ J/m^2.

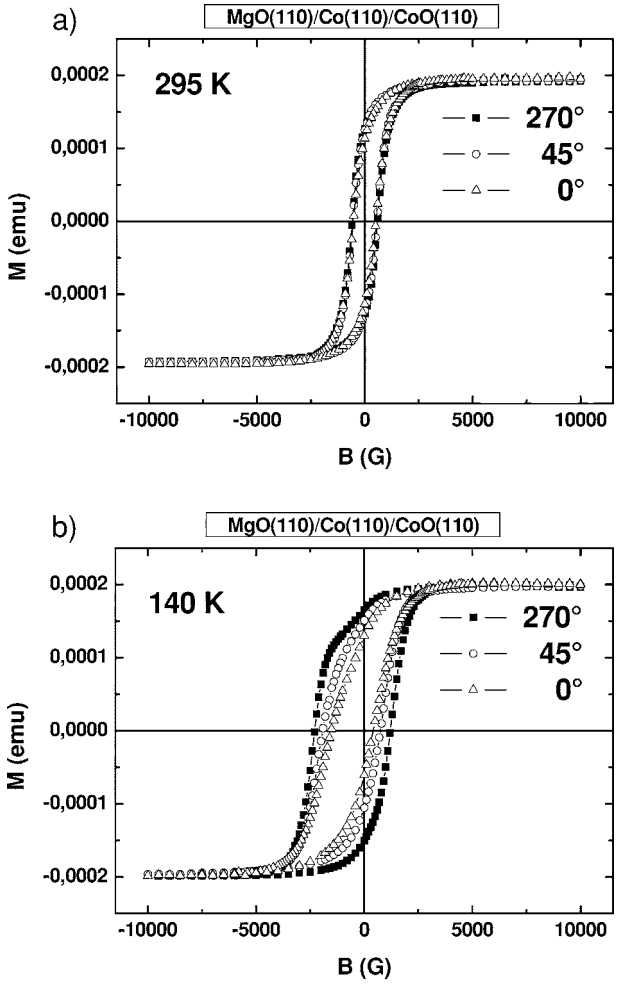

FIG. 2. Hysteresis loops measured by SQUID in the MgO(110)/Co(6 nm)/CoO(20 nm) sample. Experiments at (a) 293 K and (b) 140 K were done at the angle positions of 0°, 45°, and 270°. The 45° orientation is equivalent to the field cooling direction. The 0° and 270° orientations are equivalent to hard directions.

tropy fields, their symmetry and modifications, after the field-cooling process were as follows: the substrate crystallographic symmetry, the layer deposition sequence, twinning and the domain structure of CoO controlled by a dilution, the directional distortions at the FM/AFM interface, and the lattice mismatch between Co and CoO. The BLS technique was especially useful for probing nondestructively these effects confined within the exchange-biased Co/CoO films.

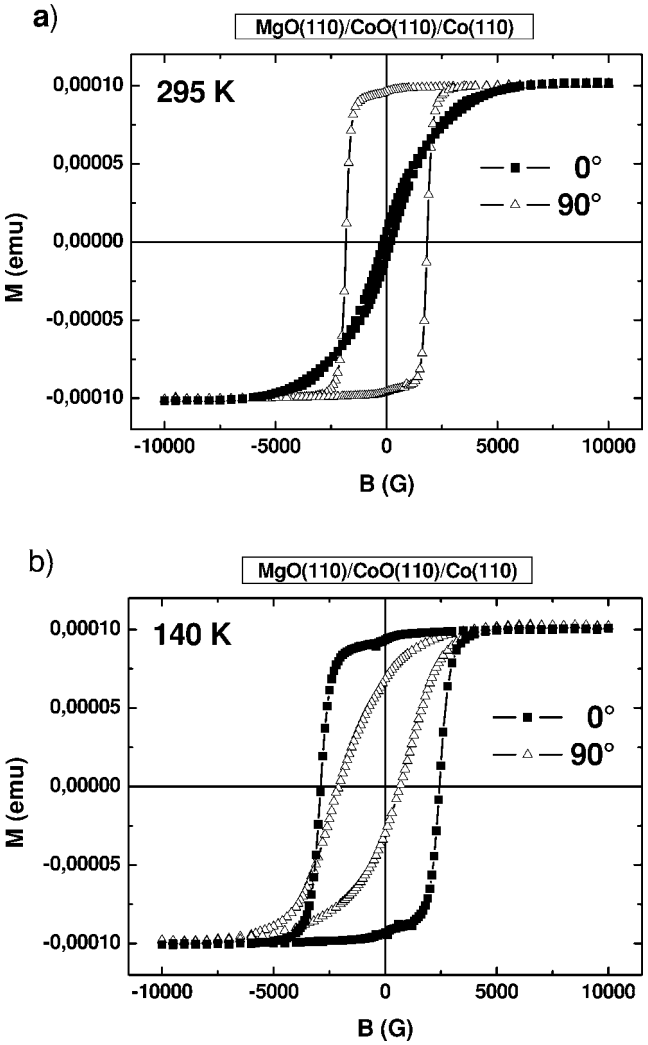

FIG. 3. Hysteresis loops measured by SQUID in the MgO(110)/CoO(20 nm)/Co(6 nm) sample revealing the switching of the anisotropy axes. Experiments at (a) 293 K and (b) 140 K were done at the position of easy axis of magnetization (90°) and in the hard axis direction perpendicular to it (0°).

ACKNOWLEDGMENT

The first author (T.B.) acknowledges DAAD for financial support during research visits at RWTH Aachen (Germany).

[1] B. Dieny, V. S. Speriosu, S. Metin, S. S. Parkin, B. A. Gurney, P. Baumgart, and D. R. Wilhoit, J. Appl. Phys. **69**, 4774 (1991).
[2] S. X. Wang, W. E. Bailey, and C. Sürgers, IEEE Trans. Magn. **33**, 2369 (1997).
[3] T. J. Gafron, S. L. Burkett, and S. E. Russek, IEEE Trans. Magn. **36**, 2611 (2000).
[4] S. Kaka, J. P. Nibarger, S. E. Russek, N. A. Stutzke, and S. L. Burkett, J. Appl. Phys. **93**, 7539 (2003).
[5] W. H. Meiklejohn and C. P. Bean, Phys. Rev. **102**, 1413 (1956); **105**, 904 (1957).
[6] J. Nogués and I. K. Schuller, J. Magn. Magn. Mater. **192**, 203 (1999).
[7] A. E. Berkowitz and K. Takano, J. Magn. Magn. Mater. **200**, 552 (1999).

[8] M. Kiwi, J. Magn. Magn. Mater. **234**, 584 (2001).
[9] B. Beschoten, A. Tillmanns, J. Keller, G. Güntherodt, U. Nowak, and K. D. Usadel, Adv. Solid State Phys. **42**, 419 (2002).
[10] U. Nowak, K. D. Usadel, J. Keller, P. Miltényi, B. Beschoten, and G. Güntherodt, Phys. Rev. B **66**, 14430 (2002).
[11] J. Keller, P. Miltényi, B. Beschoten, G. Güntherodt, U. Nowak, and K. D. Usadel, Phys. Rev. B **66**, 14431 (2002).
[12] T. Mewes, R. Lopusnik, J. Fassbender, B. Hillebrands, M. Jung, D. Engel, A. Ehresmann, and H. Schmoranzer, Appl. Phys. Lett. **76**, 1057 (2000).
[13] A. Ehresmann, D. Junk, D. Engel, A. Paetzold, and K. Röll, J. Phys. D **38**, 801 (2005).
[14] A. Ehresmann, D. Engel, T. Weis, A. Schindler, D. Junk, J. Schmalhorst, V. Höink, M. D. Sacher, and G. Reiss, Phys. Status Solidi B **243**, 29 (2006).
[15] R. D. McMichael, M. D. Stiles, P. J. Chen, and W. F. Egelhoff, Jr., Phys. Rev. B **58**, 8605 (1998).
[16] M. D. Stiles and R. D. McMichael, Phys. Rev. B **59**, 3722 (1999).
[17] P. Miltényi, Ph.D. thesis, RWTH Aachen, 2000.
[18] T. Blachowicz and M. H. Grimsditch, *Inelastic scattering technique—Brillouin, in Encyclopedia of Condensed Matter Physics*, edited by G. Bassani, G. Liedl, and P. Wyder (Elsevier, London, 2005).
[19] R. Mock, B. Hillebrands, and R. Sandercock, J. Phys. E **20**, 656 (1987).
[20] T. Błachowicz, *Brillouin Spectroscopy in Crystal Lattices. Acoustic and Spin Waves* (Silesian University of Technology Press, Gliwice 2003), pp. 102–109.
[21] B. Hillebrands, P. Baumgart, and G. Güntherodt, Phys. Rev. B **36**, 2450 (1987).
[22] C. Mathieu, M. Bauer, B. Hillebrands, J. Fassbender, G. Güntherodt, R. Jungblut, J. Kohlhepp, and A. Reinders, J. Appl. Phys. **83**, 2863 (1998).
[23] T. J. Moran, J. Nogués, D. Lederman, and I. K. Schuller, Appl. Phys. Lett. **72**, 617 (1998).
[24] A. Hoffmann, M. Grimsditch, J. E. Pearson, J. Nogués, W. A. A. Macedo, and I. K. Schuller, Phys. Rev. B **67**, 220406(R) (2003).
[25] D. Hermann-Ronzaud, P. Burlet, and J. Rossat-Mignod, J. Phys. C **11**, 2123 (1978).
[26] H. Fritzsche, J. Kohlhepp, and U. Gradmann, Phys. Rev. B **51**, 15933 (1995).
[27] O. Madelung (Ed.), *Numerical Data and Functional Relationships in Science and Technology*, Landolt-Börnstein New Series, Group III, Vol. 17b (Springer Verlag, Berlin, 1982).
[28] *Numerical Data and Functional Relationships in Science and Technology*, edited by O. Madelung, Landolt-Börnstein New Series, Group III, Vol. 17g (Springer Verlag, Berlin, 1984).
[29] N. C. Tombs and H. P. Rooksby, Nature (London) **165**, 442 (1950).
[30] S. Greenwald, J. Appl. Crystallogr. **6**, 396 (1953).
[31] *Numerical Data and Functional Relationships in Science and Technology*, edited by O. Madelung, Landolt-Börnstein New Series, Group III, Vol. 24a (Springer Verlag, Berlin, 1998).
[32] R. D. McMichael, C. G. Lee, M. D. Stiles, F. G. Serpa, P. J. Chen, and W. F. Egelhoff, J. Appl. Phys. **87**, 6404 (2000).